Supplemental Material: Micropattern-controlled wicking enhancement in hierarchical micro/nanostructures

Arif Rokoni, Dong-Ook Kim, and Ying Sun*

Department of Mechanical Engineering and Mechanics, Drexel University, Philadelphia

A. Wicking dynamics on nanostructured surfaces

To understand whether there are any nanoscale effects, such as disjoining pressure, on wicking dynamics of nanostructures, vertical wicking tests of DI water were performed using ZnO nanorods grown on a glass substrate of varying growth time and chemical concentration to achieve different nanostructure roughness.[1] Growth time of 2 to 5 hours and chemical concentration of 0.01M to 0.05M result in roughness, r_n, of 3.77 to 4.21. Figure S1 shows the wicking length, a, over time, t, for four different nanorod substrates with varying roughness, together with $a \sim t^{1/2}$ power law. The results of wicking experiments with nanostructures show good agreement with the classical $a \sim t^{1/2}$ theory, consistent with previously reported hemi wicking of water droplets on nanostructured surfaces.[2-6] For the roughness range considered, the propagation coefficient is approximated to be 0.75 mm/s$^{1/2}$ from least square fitting of all experimental data. This implies that, for the cases considered, nanoscale effects such as disjoining pressure or distorted meniscus shape have negligible effects on wicking dynamics of nanostructures.

* Corresponding author. Tel.: +1(215)895-1373; Fax: +1(215)895-1478; E-mail:ysun@coe.drexel.edu.

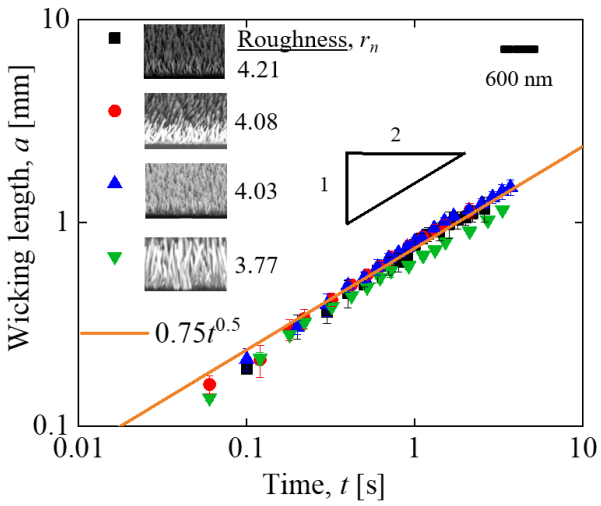

Figure S1: Wicking length versus time for vertical wicking of DI water on ZnO nanorod substrates of varying nanoscale roughness r_n of 3.77 to 4.21.

B. Wicking index on micro and hierarchical micro/nanostructured surfaces

Figure S2 shows the wicking index, *n*, over diameter-to-spacing ratio, *d/s*, for micropillars and hierarchical surfaces with micropillar height of 8μm, 13μm, 18μm, and 26μm. For all cases, the wicking indices are found to vary from 0.46 to 0.59. No clear trend of wicking index, *n*, over diameter-to-spacing ratio and height of micropillars has been found for both micropillars and hierarchical surfaces, as shown in Fig. S2. The average wicking indices for different spacings and heights of micropillars for both micropillars and hierarchical surfaces slightly deviate from 0.5 due to possible contamination of DI water and substrates during wicking and limited wicking length due to imaging size. It is noted that a wicking index of 0.5 has been considered by others for wicking in micropillars[7-10] and for wicking in hierarchical surfaces.[11]

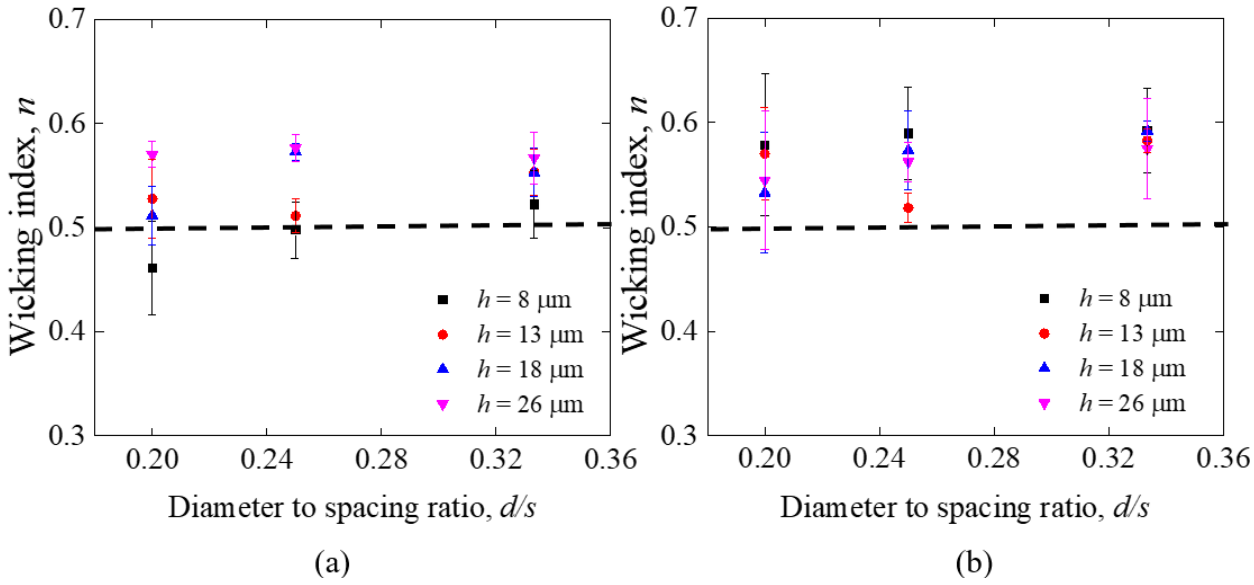

Figure S2. Wicking index over diameter-to-spacing ratio for (a) micro and (b) hierarchical surfaces. Experimental error bars are from 5 independent wicking tests of a single case.

C. Comparison of wicking on micropillar surfaces with existing wicking models

Wicking tests have been conducted on micropillars of varying diameter-to-spacing ratios and heights and the results are compared with existing closed-form models to check whether these closed-form models can predict the propagation coefficient for micropillars of the present study. For micropillars of diameter 10 μm, the center-to-center spacing varies from 30 μm to 60 μm, resulting in diameter-to-spacing ratio, *d/s*, of 0.333 to 0.167 and the height varies from 8 μm to 26 μm. Table S1 summarizes the existing closed-form models with propagation coefficients, *G*, expressed in terms of surface tension, viscosity and geometrical parameters for structured surfaces. Once the surface tension and viscosity of the wicking liquid are known, the expressions for the propagation coefficient listed in Table S1 can predict the wicking dynamics for structured surfaces having different geometrical parameters.

Table S1. Summary of existing closed-form models of wicking on structured surfaces.

Model	Propagation coefficient, G
Ishino et al.[8]	$\sqrt{\frac{2}{3}\frac{\gamma h}{\eta}\left[\cos\theta(r_m-\phi_m)-(1-\phi_m)\right]}$; $h < s$ (I) and $\sqrt{\frac{\gamma d}{\eta}(\ln(\frac{s}{d})-1.31)}$; $h > s$ considering $\theta = 0°$
Mai et al.[12]	$\sqrt{\frac{2\gamma h}{3\mu\beta}\frac{\cos\theta-\cos\theta_c}{\cos\theta_c}}$; $\beta=\frac{4h^2}{w^2}+1$; $w=\left[s^2-\left(\frac{\pi}{4}d^2\right)\right]/s$ (II)
Kim et al.[10]	$0.49\sqrt{\frac{[\cos\theta(r_m-\phi_{s,m})-(1-\phi_{s,m})]}{1+\frac{h(r_m-1)}{S-d}}\frac{\gamma h}{\mu}}$; $r_m=1+\frac{\pi dh}{s^2}$; $\phi_{s,m}=\frac{\pi d^2}{4s^2}$ (III)
Present study	$0.35\sqrt{\frac{\left(r_m-\phi_{s,m}\right)\cos\theta-(1-\phi_{s,m})}{1-\frac{d}{s}\left(1-\frac{d}{s}\right)+\frac{d}{s}\left((r_m-1)\frac{h}{(s-d)}\right)}\frac{\gamma h}{\mu}}$ (IV)
Here, d, s and h are the diameter, spacing and height of micropillars, γ and η are the surface tension and viscosity of DI water, w is the width of the channel, where wicking in micropillars is simplified as wicking in channels of the same porosity[12]. θ and θ_c are the intrinsic contact angle and critical contact angle of wicking, respectively, and $\cos\theta_c=\frac{1-\phi_{s,m}}{r_m-\phi_{s,m}}$, where r_m and $\phi_{s,m}$ are roughness and solid fraction of micropillars. The propagation coefficient of 0.49 in Eq. (III) is for dense pillar arrangements, and for spare pillar arrangement it is < 0.49. Equation (IV) from the present model is obtained from Eq. (8) of the main text with an empirically determined constant 0.35.	

Figure S3 shows the comparison of experimentally determined propagation coefficients with the existing closed-form models of Ishino et al.[8], Mai et al.[12], Kim et al.[10], and the present study, Eq. (8) of the main text, for varying diameter-to-spacing ratios for micropillar heights of 18 and 26 μm. For both pillar heights, the model of Ishino et al.[8] overpredicts the propagation coefficient due to neglecting the friction from the pillars and the discrepancy increases with the

diameter-to-spacing ratio. The model of Mai et al.[12], where pillar arrays are considered as channels having the same porosity keeping height and length of the channel the same as those of circular pillars, also overpredicts the propagation coefficient for the diameter-to-spacing ratios considered. Interestingly, the model proposed by Kim et al.[10] agrees well with the experimental results over the range of micropillar diameter-to-spacing ratios for both heights of the micropillars. Kim et al.[10] model considers the flow profiles in two regions, around the pillars (bounded by pillar sidewalls and bottom surface) and in between pillars (bounded by bottom surface), and a two-stage wicking motion is observed for sparse pillars where the propagation coefficient is smaller than 0.49. As discussed in Sec. 3 of the main text, this two-stage motion is also observed in the present study for wicking in micropillars with diameter-to-spacing ratios of 0.2 to 0.33. For both micropillar heights of 18 and 26 μm, the present model agrees very well with experiments for *d/s* ratio of 0.16 to 0.33.

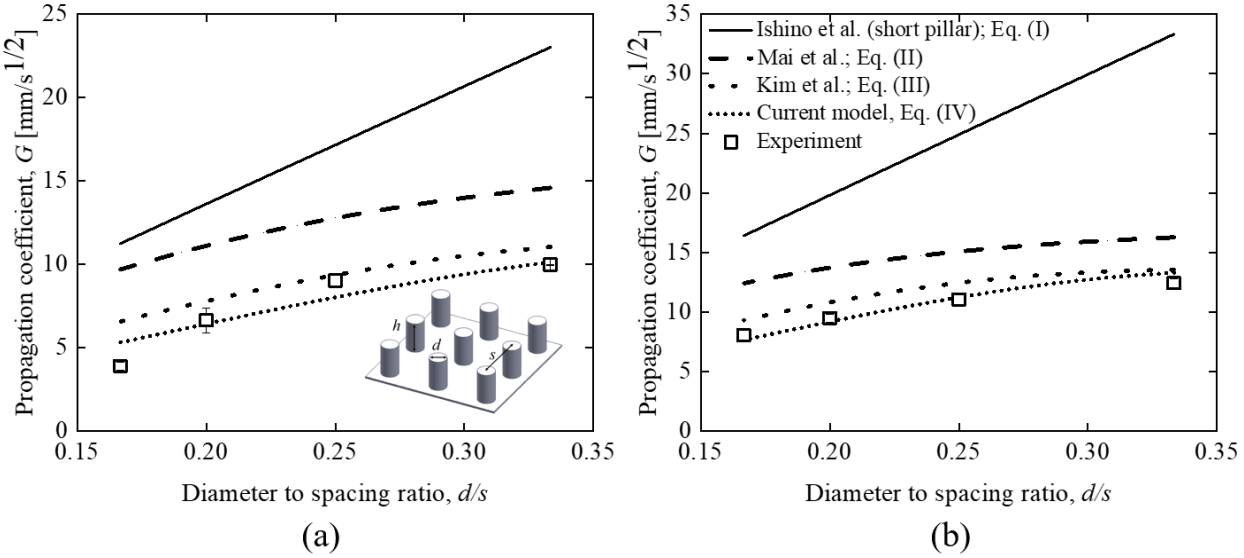

Figure S3. Comparison of micropillar wicking experiments with the existing closed-form models for different diameter-to-spacing ratios at the pillar height of (a) h=18 μm and (b) h=26 μm. Experimental error bars are from 5 independent wicking tests of a single case.

References

1. Baxter, J. B.; Walker, A.; Van Ommering, K.; Aydil, E., Synthesis and characterization of ZnO nanowires and their integration into dye-sensitized solar cells. *Nanotechnology* **2006,** *17* (11), S304.
2. Wemp, C. K.; Carey, V. P., Water wicking and droplet spreading on randomly structured thin nanoporous layers. *Langmuir* **2017,** *33* (50), 14513-14525.
3. Chen, X.; Chen, J.; Ouyang, X.; Song, Y.; Xu, R.; Jiang, P., Water droplet spreading and wicking on nanostructured surfaces. *Langmuir* **2017,** *33* (27), 6701-6707.
4. Fan, J.-G.; Zhao, Y.-P., Spreading of a water droplet on a vertically aligned Si nanorod array surface. *Applied physics letters* **2007,** *90* (1), 013102.
5. Kim, B. S.; Lee, H.; Shin, S.; Choi, G.; Cho, H. H., Interfacial wicking dynamics and its impact on critical heat flux of boiling heat transfer. *Applied Physics Letters* **2014,** *105* (19), 191601.
6. Quan Lai, C.; Thi Mai, T.; Zheng, H.; Lee, P.; Leong, K.; Lee, C.; Choi, W., Influence of nanoscale geometry on the dynamics of wicking into a rough surface. *Applied Physics Letters* **2013,** *102* (5), 053104.
7. Nam, Y.; Sharratt, S.; Byon, C.; Kim, S. J.; Ju, Y. S., Fabrication and characterization of the capillary performance of superhydrophilic Cu micropost arrays. *Journal of Microelectromechanical Systems* **2010,** *19* (3), 581-588.
8. Ishino, C.; Reyssat, M.; Reyssat, E.; Okumura, K.; Quere, D., Wicking within forests of micropillars. *EPL (Europhysics Letters)* **2007,** *79* (5), 56005.
9. Xiao, R.; Enright, R.; Wang, E. N., Prediction and optimization of liquid propagation in micropillar arrays. *Langmuir* **2010,** *26* (19), 15070-15075.
10. Kim, J.; Moon, M.-W.; Kim, H.-Y., Dynamics of hemiwicking. *Journal of Fluid Mechanics* **2016,** *800*, 57-71.
11. Wang, Z.; Zhao, J.; Bagal, A.; Dandley, E. C.; Oldham, C. J.; Fang, T.; Parsons, G. N.; Chang, C.-H., Wicking enhancement in three-dimensional hierarchical nanostructures. *Langmuir* **2016,** *32* (32), 8029-8033.
12. Mai, T. T.; Lai, C. Q.; Zheng, H.; Balasubramanian, K.; Leong, K.; Lee, P.; Lee, C.; Choi, W., Dynamics of wicking in silicon nanopillars fabricated with interference lithography and metal-assisted chemical etching. *Langmuir* **2012,** *28* (31), 11465-11471.